Acta Oceanol. Sin., 2018, Vol. 37, No. 11, P. 61–67
DOI: 10.1007/s13131-018-1333-y
http://www.hyxb.org.cn
E-mail: hyxbe@263.net

Newly discovered hydrothermal fields along the ultraslow-spreading Southwest Indian Ridge around 63°E

CHEN Jie[1], TAO Chunhui[1]*, LIANG Jin[1], LIAO Shili[1], DONG Chuanwan[1, 2], LI Huaiming[1], LI Wei[1], WANG Yuan[1], YUE Xihe[1, 3], HE Yonghua[1]

[1] Key Laboratory of Submarine Geosciences, Second Institute of Oceanography, State Oceanic Administration, Hangzhou 310012, China

[2] School of Earth Sciences, Zhejiang University, Hangzhou 310010, China

[3] College of Marine Science and Technology, China University of Geoscience, Wuhan 430074, China

Received 5 May 2018; accepted 8 June 2018

Abstract

The ultraslow-spreading Southwest Indian Ridge (SWIR) to the east of the Melville fracture zone is characterized by very low melt supply and intensive tectonic activity. Due to its weak thermal budget and extremely slow spreading rate, the easternmost SWIR was considered to be devoid of hydrothermal activity until the discovery of the inactive Mt. Jourdanne hydrothermal field (27°51′S, 63°56′E) in 1998. During the COMRA DY115-20 cruise in 2009, two additional hydrothermal fields (i.e., the Tiancheng (27°51′S, 63°55′E) and Tianzuo (27°57′S, 63°32′E) fields) were discovered. Further detailed investigations of these two hydrothermal sites were conducted by Chinese manned submersible *Jiaolong* in 2014–2015. The Tiancheng filed can be characterized as a low-temperature (up to 13.2°C) diffuse flow hydrothermal field, and is hosted by fractured basalts with hydrothermal fauna widespread on the seafloor. The Tianzuo hydrothermal field is an inactive sulfide field, which is hosted by ultramafic rocks and controlled by detachment fault. The discovery of the three hydrothermal fields around Segment #11 which receives more melt than the regional average, provided evidence for local enhanced magmatism providing heat source to drive hydrothermal circulation. We further imply that hydrothermal activity and sulfide deposits may be rather promising along the easternmost SWIR.

Key words: Southwest Indian Ridge, ultraslow-spreading, hydrothermal field, local enhanced magmatism, heat source

Citation: Chen Jie, Tao Chunhui, Liang Jin, Liao Shili, Dong Chuanwan, Li Huaiming, Li Wei, Wang Yuan, Yue Xihe, He Yonghua. 2018. Newly discovered hydrothermal fields along the ultraslow-spreading Southwest Indian Ridge around 63°E. Acta Oceanologica Sinica, 37(11): 61–67, doi: 10.1007/s13131-018-1333-y

1 Introduction

Seafloor polymetallic sulfides are rich in elements such as Fe, Cu, Zn, Au and Ag, and they are widely found along the mid-ocean ridges (MORs), arcs and back-arc basins (Baker, 2017). It is estimated that the total accumulation of sulfides in these areas is on the order of 6×10^8 tons, which contained about 3×10^7 tons of copper and zinc. This is equivalent to that of the massive sulfide deposits formed during the Cenozoic Era on land (Hannington et al., 2011). Therefore, seafloor polymetallic sulfides should be considered highly valuable as a potentially strategic metallic resource in the future.

Polymetallic sulfides are the products of seafloor hydrothermal activities. According to the latest database from InterRidge (http://www.interridge.org/), more than 680 hydrothermal vent fields or anomalies have been found worldwide, and more than half of them occur along the MORs. In the last three decades, investigations of seafloor hydrothermal vent fields have been conducted along MORs, primarily focused on the fast-spreading East Pacific Rise (e.g., Haymon et al., 1991; Baker et al., 1994), the intermediate-spreading Southeast Indian Ridge (e.g., Scheirer et al., 1998; Baker et al., 2014), the slow-spreading Mid-Atlantic Ridge (e.g., Rona et al., 1986; Tao et al., 2017) and the Central Indian Ridge (e.g., Pluger et al., 1990; Son et al., 2014).

The ultraslow-spreading (full spreading rate <20 mm/a) Southwest Indian Ridge (SWIR) and Arctic ridges, which account for more than 20% of the total length of the MORs, have also been investigated during the last 20 years (e.g., German et al., 1998; Münch et al., 2001; Bach et al., 2002; Edmonds et al., 2003; Baker et al., 2004; Tao et al., 2012). However, only approximately 40 hydrothermal fields/anomalies have been found along these two ridges, accounting for 10% of the total number of hydrothermal fields along the MORs (data from InterRidge).

The easternmost SWIR (full spreading at 12–14 mm/a), to east of the Melville fracture zone, is characterized by very low melt supply with a relatively low mantle temperature and thin crust (e.g., Cannat et al., 1999, 2003; Seyler et al., 2003; Minshull et al., 2006; Sauter et al., 2013). Due to its weak thermal budget and extremely slow spreading rate, this portion was considered devoid of hydrothermal activity (Baker et al., 1996). The earliest evidence of hydrothermal activity in this area (Plume 5 and Plume 6

Foundation item: The National Key Research and Development Program of China under contract Nos 2017YFC0306603, 2018YFC0309901, 2016YFC0304905, 2017YFC0306803 and 2018YFC0309902; the China Ocean Mineral Resources Research and Development Association Major Project under contract Nos DY135-S1-1-01 and DY135-S1-1-02.
*Corresponding author, E-mail: taochunhuimail@163.com

in Fig. 1a) was the detection of water-column anomalies obtained in 1997 during the FUJI cruise (German et al., 1998). During the INDOYO cruise with submersible *Shinkai 6500* in 1998, the inactive Mt. Jourdanne hydrothermal field located at 27°51′S, 63°56′E was discovered, and samples of massive sulfide and chimney were collected (Münch et al., 2001). This evidence suggests that hydrothermal activities do exist in the easternmost SWIR.

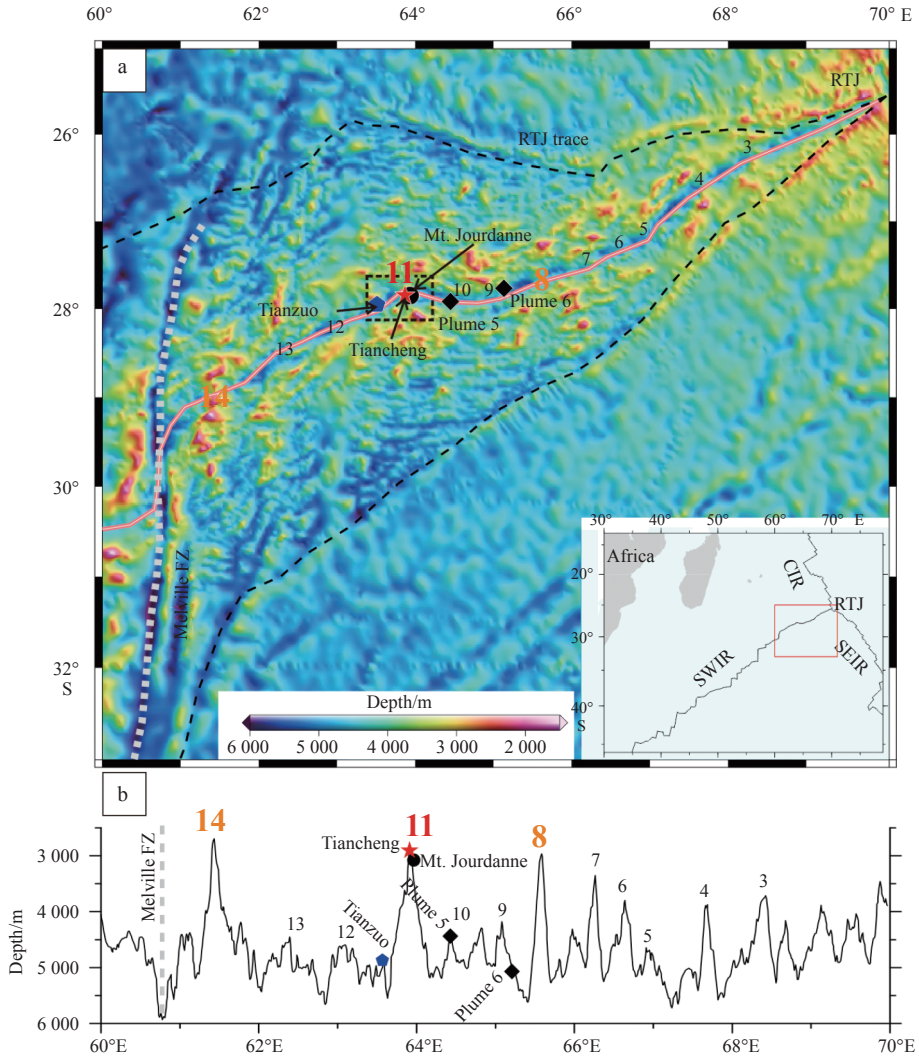

Fig. 1. Satellite-derived topographic map (a) and along-axis bathymetric profile (b) of the Southwest Indian Ridge (SWIR) between 60°E and 70°E. On the topographic map (a), Plume 5 and Plume 6, hydrothermal water-column anomalies, are marked by black diamonds. The Mt. Jourdanne hydrothermal field is marked by a black circle. The Tiancheng and Tianzuo hydrothermal fields are marked by a red star and a blue pentagon, respectively. The black dotted box shows the areas shown detailed by the bathymetric map in Fig. 2. The segments cited in the text and/or in other figures are identified by their number, following the nomenclature of Cannat et al. (1999). RTJ: Rodrigues Triple Junction; Melville FZ: Melville fracture zone; CIR: Central Indian Ridge; SEIR: Southeast Indian Ridge. The bathymetric profile (b) shows the location and water depth of the Plume 5, Plume 6, Mt. Jourdanne, Tiancheng and Tianzuo hydrothermal fields, based on bathymetric data collected by Patriat et al. (1997). It is notable that Segments #8, #11 and #14 all have a relief of more than 2 km.

Two additional hydrothermal fields, named the Tiancheng (27°51′S, 63°55′E) and Tianzuo (27°57′S, 63°32′E), were discovered around 63°E during the COMRA DY115-20 cruise conducted by R/V *Dayang Yihao* in 2009 (Tao et al., 2014). Further detailed investigations of these two hydrothermal sites were carried out by Chinese manned submersible *Jiaolong* during the COMRA DY115-35 cruise conducted by R/V *XiangYang Hong 9* in 2014–2015. According to the investigations from the R/V *Dayang Yihao* and the direct observations during the *Jiaolong* 87th and 88th dives, the geological and environmental characteristics of Tiancheng and Tianzuo hydrothermal fields are described in detail. In addition, details pertaining to the formation of the hydrothermal fields are also provided.

2 Geological setting

Between the Bouvet (0°E) and Rodriguez (70°E) Triple Junctions, the SWIR is the divergent plate boundary between the Antarctic and Nubian/Somalian plates with a total length of 7 700 km. The SWIR is among the world's ultraslow spreading ridges with a full spreading rate of 12–18 mm/a (Dick et al., 2003;

Horner-Johnson et al., 2005). At such a slow spreading rate, the lithosphere of the SWIR is thicker and colder than faster spreading ridges, then the effect of conductive cooling reducing the melt supply and enhancing tectonics (Cannat et al., 1999; Dick et al., 2003; Standish and Sims, 2010; Hebert and Montési, 2010).

The easternmost SWIR is at an angle of approximately 60° to the spreading direction, over which no transform fault is observed (Fig. 1a). This part of the SWIR represents a melt-poor endmember of the MOR system, supported by bathymetric, side-scan sonar imagery, gravity, seismic and geochemical data (Meyzen et al., 2003; Seyler et al., 2003; Cannat et al., 2006; Minshull et al., 2006; Sauter et al., 2013; Momoh et al., 2017). Near-bottom sonar images indicated intensive tectonism with exhumation and widespread exposure of mantle rocks (Sauter et al., 2013). The long-lived detachment faults, which dip into the lower crust and extend to the surface, accommodate most of the plate separation (Cannat et al., 2003; Sauter et al., 2013; Smith, 2013). However, several magmatic segments with high relief (i.e., Segments #8, #11 and #14) were observed along the easternmost SWIR (Fig. 1b). In general, these segments display a volcanic structure, and are several tens of meters high with a lateral extension of several tens of kilometers. Accordingly, they are considered to be ideal for hydrothermal activity and the formation of sulfide deposits (Münch et al., 2001; Baker et al., 2004).

The Tiancheng, Tianzuo and Mt. Jourdanne hydrothermal fields are located at Segment #11 (Fig. 2). This segment has an hourglass shape that extends more than 20 km in the north-south direction, and has an axial volcanic ridge (AVR) bounded in the east and the west by nontransform discontinuities (NTDs). The AVR is approximately 300 m high with the peak reaching a water depth of about 2 670 m. The along-axis variations of topography and mantle Bouguer anomaly (MBA) of Segment #11 is estimated to be approximately 2 700 m and 53 mGal, respectively, which suggests that the melt supply must be focused beneath the segment center, decreasing toward the segment ends (Cannat et al., 1999). On the other hand, the crustal thickness is more than 6 km under the center of the high relief Segment #11, corresponding to a negative residual MBA (RMBA), whereas the maximum crustal thicknesses under adjacent segments (i.e., Segments #9 and #10) are only 2–3 km thick (Fig. 3) (Cannat et al., 2003). Melt distribution around Segment #11 is therefore high and focused, which may be dominated by a strong melt-focusing process, similar to other strong melt-focusing segments along the SWIR (e.g., Segments 14, 20–22 and PE-1) (Cannat et al., 1999; Sauter et al., 2001; Sato et al., 2013).

3 Hydrothermal fields with submersible observations

3.1 *Tiancheng low-temperature diffuse flow filed*

The Tiancheng hydrothermal field is located at the center of Segment #11 with a water depth of 2 750 m, and is situated to the west of the inactive sulfide field Mt. Jourdanne with a water depth of 2 950 m (Fig. 4). The Tiancheng field was detected by water temperature and turbidity anomalies with hydrothermal mussels and crabs during the COMRA DY115–20 cruise (Tao et al., 2014). During the *Jiaolong* 87th dive, the main outcrop of the field was confirmed and is characterized by basaltic rocks (Fig. 5a). The summit of Mt. Jourdanne is also characterized by a series of extrusive units (Münch et al., 2001), principally alternating sheet flows, lobate flows, tubes, and pillow basalts, which comprise the main outcrop of the northeastern part of the AVR. In the underwater view, basaltic rocks were generally fractured by surface faults and fissures (Figs 5b and c). The Tiancheng field is a low-temperature (low–*T*) diffuse flow hydrothermal field, with temperatures measured up to 13.2°C (Figs 5d and e). Numerous hydrothermal animals were observed on and around the diffuse vent, with a distribution range of 70–100 m in diameter from the vent, including mussels, gastropods, crabs, shrimps, barnacles and anemones (Figs 5b, c and d), indicating a possibility of nearby high-temperature hydrothermal activities. Many hydro-

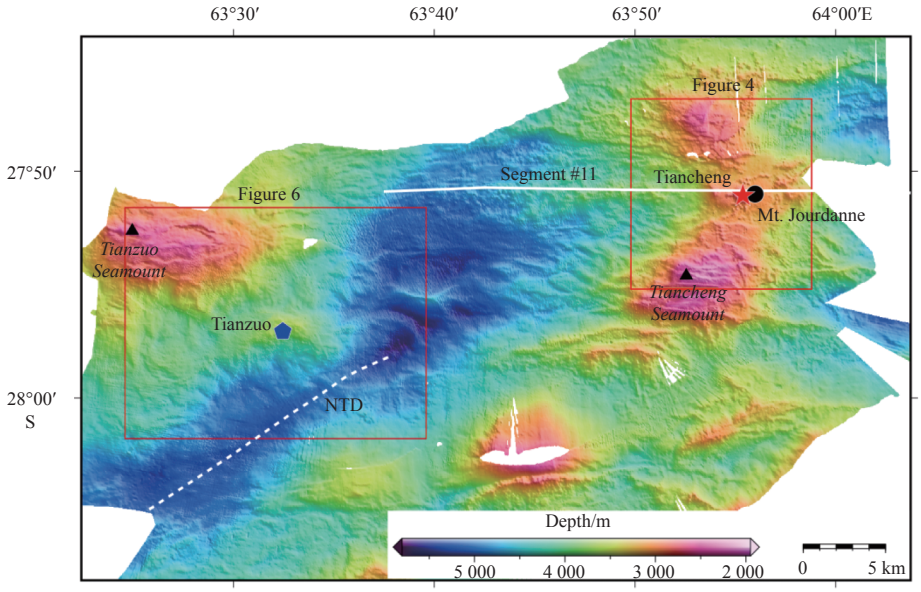

Fig. 2. Bathymetric map between 63°20′E and 64°10′E. White solid and dashed lines indicate the axes of Segment #11 and nontransform discontinuity (NTD), respectively. The Tiancheng and Mt. Jourdanne hydrothermal fields, located at the center of Segment #11, are marked by a red star and a black circle, respectively. The Tianzuo hydrothermal field, close to NTD, is marked by a blue pentagon. The Tiancheng and Tianzuo Seamounts are marked by black triangles. The red boxes denote the areas shown in the three-dimensional views presented in Figs 4 and 6, respectively

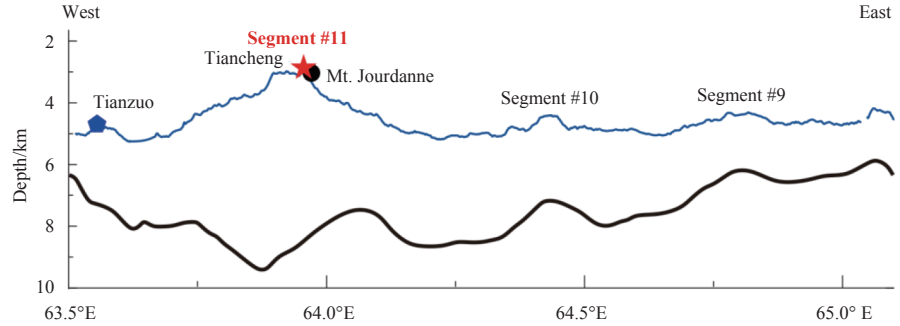

Fig. 3. Along-axis topography and Moho depth of Segments #9, #10 and #11 presented in Fig. 1 (Cannat et al., 2003). Blue line represents topography and thick black line represents the Moho depth, as predicted from gravity. Three confirmed hydrothermal fields are marked in the Figure. The Tiancheng and Mt. Jourdanne hydrothermal fields, which are characterized by thicker crust, are marked by a red star and a black circle, respectively. The Tianzuo hydrothermal field is marked by a blue pentagon and is characterized by a thin crust.

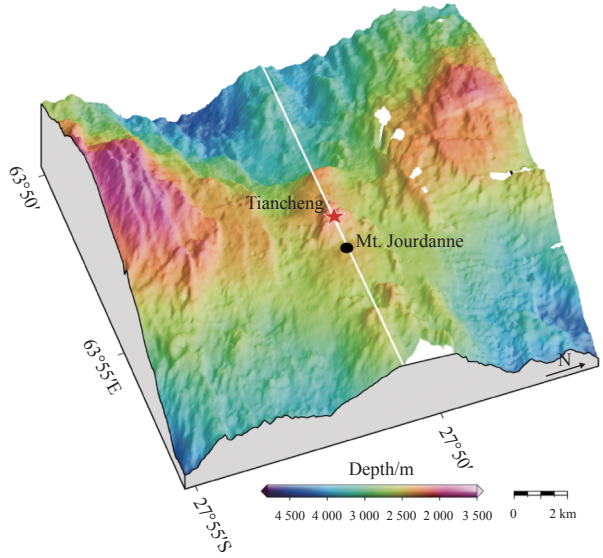

Fig. 4. Three-dimensional view around the Tiancheng and Mt. Jourdanne hydrothermal fields, viewed from the SSE with a vertical exaggeration of 2. The white line indicates the segment axis. The red star indicates the location of the Tiancheng hydrothermal field and the *Jiaolong* 87th dive. The black circle indicates the location of the Mt. Jourdanne hydrothermal field.

thermal fields, such as TAG and Longqi fields, include both high-temperature vents in the center and low-temperature vents near the perimeter (Lalou et al., 1995; Tao et al., 2012). The low-temperature hydrothermal products (opal) were locally observed (Fig. 5f).

3.2 *Tianzuo inactive sulfide field*

The Tianzuo hydrothermal field is located at approximately 14 km southeast to the Tianzuo Seamount, with a water depth of 3 630 m (Fig. 6). It is situated on the top of a dome-shape structure, which is a typical architecture associated with oceanic detachment faults. The hydrothermal activity of the Tianzuo field is supposed to be controlled by the detachment fault, similar to Logatchev and Rainbow hydrothermal fields along the Mid-Atlantic Ridge (MAR) (German et al., 1996; Schmidt et al., 2007). During the *Jiaolong* 88th dive, the main outcrop of the Tianzuo field was characterized by altered ultramafic rocks and hydrothermal precipitates (Figs 7a and b), with no significant signs of activity or no typical vent fauna. These alterated ultramafic rocks were serpentinized iherzolite, which primarily contain olivine, pyroxene, and their alterated serpentine (Tao et al., 2014). The opal and red-brown sediments were widely observed on the sea floor with a distribution range of approximately 800 m×530 m, and the surface massive sulfides showed significant weathering, and the seafloor outside the field is covered by thick sediments (Figs 7b, c and d), indicating that the ancient hydrothermal activity have ceased for a long time. Samples of the massive sulfide, collected during DY115–20 cruise, are mainly comprised of minerals like pyrrhotite, pyrite and chalcopyrite (Tao et al., 2014). The Tianzuo hydrothermal field is therefore an inactive sulfide site which is hosted by ultramafic rocks and controlled by detachment fault along the SWIR.

4 Discussion

The easternmost SWIR is characterized by very low melt supply and tectonic processes locally accommodate almost all of the plate divergence (Sauter et al., 2013; Smith, 2013). Magmatism plays a minor role in the plate spreading of this part of the SWIR. However, the injection of small amounts of melt into the plate, local enhanced magmatism, could drive the hydrothermal circulation (Tao et al., 2012; Sauter et al., 2013). This local magmatism provides sufficient heat sources for hydrothermal circulation, and may play a primary role in controlling the distribution of hydrothermal activities at the ultraslow-spreading ridges (Baker et al., 2004; Tao et al., 2012).

The discovery of the Tiancheng, Tianzuo and Mt. Jourdanne hydrothermal fields around Segment #11 confirmed that local enhanced magmatism at the ultraslow-spreading ridges could facilitate the formation of hydrothermal activities. Segment #11 receives more melt than the regional average of the easternmost SWIR, which appears to be capable of driving hydrothermal circulation, similar to Segment #27 of the SWIR (Cannat et al., 2003; Yang et al., 2017). The Tiancheng and Mt. Jourdanne fields are located at segment center where the melt supply is most focused and basalts are widespread on the seafloor (Fig. 5a), suggesting a sufficient heat source in this area. The Tianzuo field has ceased for a long time, as supported by the observation of significantly weathered sulfides and the presences of a thick sediment layer (Figs 7b and d), implying that the heat supply may be insufficient to maintain the hydrothermal circulation of this field. This could be related to the Tianzuo field close to NTD and far from the heat

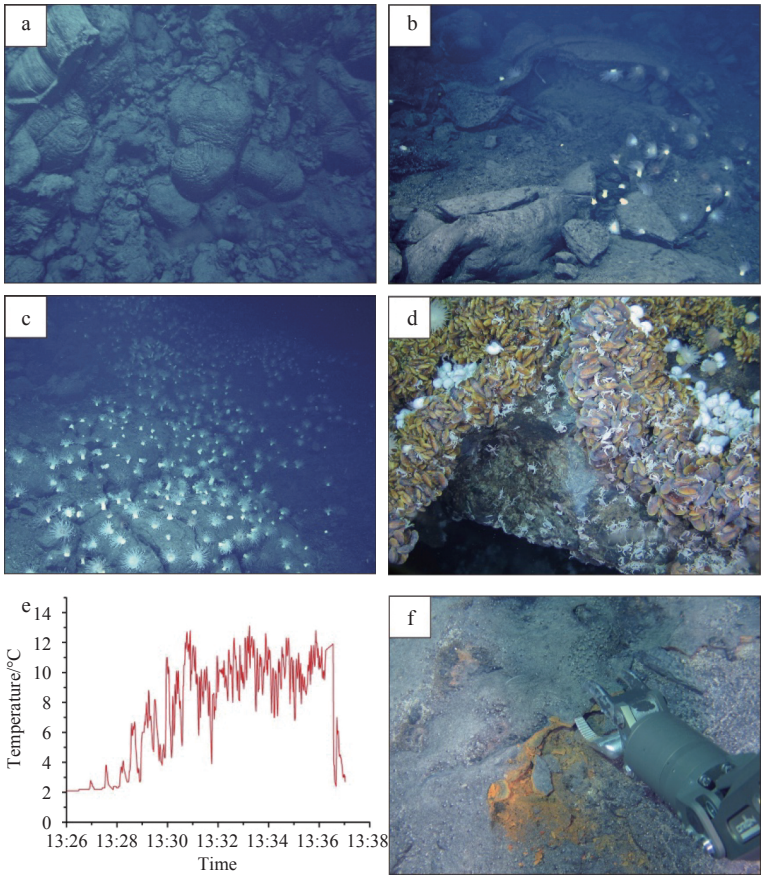

Fig. 5. *Jiaolong* 87th dive, showing seafloor features and temperature measurements at the Tiancheng hydrothermal field. a. *In situ* basaltic rocks; b. fractured basaltic rocks and hydrothermal animals; c. fault plane with widely distributed hydrothermal animals; d. dense hydrothermal animals at a diffuse flow vent; e. diffuse vent temperature (up to 13.2°C); and f. low-temperature hydrothermal products (opal). The metal sampler is the mechanical arm of *Jiaolong*.

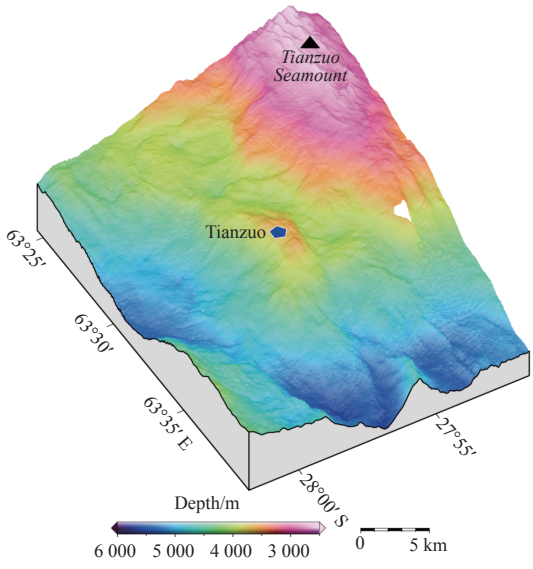

Fig. 6. Three-dimensional view around the Tianzuo hydrothermal field, viewed from the SSE with a vertical exaggeration of 2. The Tianzuo hydrothermal field is marked by a blue pentagon, situated on the top of a dome-shape structure. The black triangle indicates the location of the Tianzuo hydrothermal field and the location of the *Jiaolong* 88th dive.

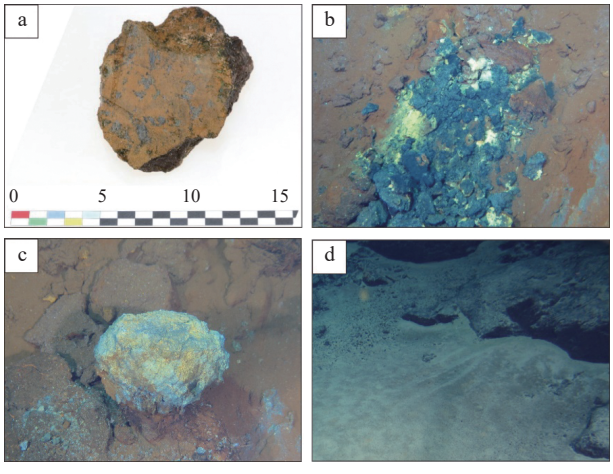

Fig. 7. *Jiaolong* 88th dive, showing seafloor features of the Tianzuo hydrothermal field. a. Ultramafic sample (highly serpentinized); b. opal, red-brown sediments, and weathered massive sulfides; c. Opal and red-brown sediments in detail; and d. thick sediments outside the Tianzuo field.

source center (center of Segment #11).

Owing to the extremely slow spreading rate, the hydrothermal system at the easternmost SWIR is generally more stable than that at faster spreading ridges (Lalou et al., 1995). The hydro-

thermal activity can be preserved for tens of thousands of years. For example, the age data of the Mt. Jourdanne indicated the hydrothermal activity lasted more 50 000 years (Münch et al., 2001). It provides favorable conditions for the formation of large sulfide deposits (Lalou et al., 1995; German et al., 2016). Furthermore, Segments #8 and #14 which are characterized by similar magmatism, might be the most promising areas of searching for new hydrothermal activities or sulfide deposits along the easternmost SWIR.

5 Conclusions

This paper reported the investigations of the Tiancheng and Tianzuo hydrothermal fields around 63°E along the SWIR during manned submersible *Jiaolong* 87th and 88th dives. The Tiancheng filed is a low-temperature diffuse flow hydrothermal field with hydrothermal fauna widespread on the seafloor. The Tianzuo hydrothermal field is an inactive sulfide field, which is hosted by ultramafic rock and controlled by detachment fault. These study results provide evidence that hydrothermal activity or sulfide deposits might be widely distributed where local enhanced magmatism drives hydrothermal circulation along the easternmost SWIR.

Acknowledgments

The authors would like to thank the captain and crew of the COMRA DY115–20 cruise on R/V *Dayang Yihao*, and the COMRA DY115–35 cruise on R/V *XiangYang Hong 9*. They would also like to thank the technical group of the submersible *Jiaolong*.

References

Bach W, Banerjee N R, Dick H J B, et al. 2002. Discovery of ancient and active hydrothermal systems along the ultra-slow spreading Southwest Indian Ridge 10°–16°E. Geochemistry, Geophysics, Geosystems, 3(7): 1044

Baker E T. 2017. Exploring the ocean for hydrothermal venting: new techniques, new discoveries, new insights. Ore Geology Reviews, 86: 55–69, doi: 10.1016/j.oregeorev.2017.02.006

Baker E T, Chen Y J, Morgan J P. 1996. The relationship between near-axis hydrothermal cooling and the spreading rate of mid-ocean ridges. Earth and Planetary Science Letters, 142(1–2): 137–145, doi: 10.1016/0012-821X(96)00097-0

Baker E T, Edmonds H N, Michael P J, et al. 2004. Hydrothermal venting in magma deserts: the ultraslow-spreading Gakkel and Southwest Indian Ridges. Geochemistry, Geophysics, Geosystems, 5(8), doi: 10.1029/2004GC000712

Baker E T, Feely R A, Mottl M J, et al. 1994. Hydrothermal plumes along the East Pacific Rise, 8°40′ to 11°50′N: plume distribution and relationship to the apparent magmatic budget. Earth and Planetary Science Letters, 128(1–2): 1–17, doi: 10.1016/0012-821X(94)90022-1

Baker E T, Hémond C, Briais A, et al. 2014. Correlated patterns in hydrothermal plume distribution and apparent magmatic budget along 2500 km of the Southeast Indian Ridge. Geochemistry, Geophysics, Geosystems, 15(8): 3198–3211, doi: 10.1002/2014GC005344

Cannat M, Rommevaux-Jestin C, Fujimoto H. 2003. Melt supply variations to a magma-poor ultra-slow spreading ridge (Southwest Indian Ridge 61° to 69°E). Geochemistry, Geophysics, Geosystems, 4(8): 9104

Cannat M, Rommevaux-Jestin C, Sauter D, et al. 1999. Formation of the axial relief at the very slow spreading Southwest Indian Ridge (49° to 69°E). Journal of Geophysical Research: Solid Earth, 104(B10): 22825–22843, doi: 10.1029/1999JB900195

Cannat M, Sauter D, Mendel V, et al. 2006. Modes of seafloor generation at a melt-poor ultraslow-spreading ridge. Geology, 34(7): 605–608, doi: 10.1130/G22486.1

Dick H J, Lin J, Schouten H. 2003. An ultraslow-spreading class of ocean ridge. Nature, 426(6965): 405–412, doi: 10.1038/nature02128

Edmonds H N, Michael P J, Baker E T, et al. 2003. Discovery of abundant hydrothermal venting on the ultraslow-spreading Gakkel ridge in the Arctic Ocean. Nature, 421(6920): 252–256, doi: 10.1038/nature01351

German C R, Baker E T, Mevel C, et al. 1998. Hydrothermal activity along the southwest Indian ridge. Nature, 395(6701): 490–493, doi: 10.1038/26730

German C R, Klinkhammer G P, Rudnicki M D. 1996. The rainbow hydrothermal plume, 36°15′N, MAR. Geophysical Research Letters, 23(21): 2979–2982, doi: 10.1029/96GL02883

German C R, Petersen S, Hannington M D. 2016. Hydrothermal exploration of mid-ocean ridges: where might the largest sulfide deposits be forming? Chemical Geology, 420: 114–126, doi: 10.1016/j.chemgeo.2015.11.006

Hannington M, Jamieson J, Monecke T, et al. 2011. The abundance of seafloor massive sulfide deposits. Geology, 39(12): 1155–1158, doi: 10.1130/G32468.1

Haymon R M, Fornari D J, Edwards M H, et al. 1991. Hydrothermal vent distribution along the East Pacific Rise crest (9°09′–54′N) and its relationship to magmatic and tectonic processes on fast-spreading mid-ocean ridges. Earth and Planetary Science Letters, 104(2–4): 513–534, doi: 10.1016/0012-821X(91)90226-8

Hebert L B, Montési L G J. 2010. Generation of permeability barriers during melt extraction at mid-ocean ridges. Geochemistry, Geophysics, Geosystems, 11(12): Q12008

Horner-Johnson B C, Gordon R G, Cowles S M, et al. 2005. The angular velocity of Nubia relative to Somalia and the location of the Nubia-Somalia-Antarctica triple junction. Geophysical Journal International, 162(1): 221–238, doi: 10.1111/gji.2005.162.issue-1

Lalou C, Reyss J L, Brichet E, et al. 1995. Hydrothermal activity on a 10^5-year scale at a slow-spreading ridge, TAG hydrothermal field, Mid-Atlantic Ridge 26°N. Journal of Geophysical Research: Solid Earth, 100(B9): 17855–17862, doi: 10.1029/95JB01858

Meyzen C M, Toplis M J, Humler E, et al. 2003. A discontinuity in mantle composition beneath the southwest Indian Ridge. Nature, 421(6924): 731–733, doi: 10.1038/nature01424

Minshull T A, Muller M R, White R S. 2006. Crustal structure of the Southwest Indian Ridge at 66°E: seismic constraints. Geophysical Journal International, 166(1): 135–147, doi: 10.1111/gji.2006.166.issue-1

Momoh E, Cannat M, Watremez L, et al. 2017. Quasi-3-D seismic reflection imaging and wide-angle velocity structure of nearly amagmatic oceanic lithosphere at the ultraslow-spreading Southwest Indian Ridge. Journal of Geophysical Research: Solid Earth, 112(12): 9511–9533

Münch U, Lalou C, Halbach P, et al. 2001. Relict hydrothermal events along the super-slow Southwest Indian spreading ridge near 63°56′E—mineralogy, chemistry and chronology of sulfide samples. Chemical Geology, 177(3–4): 341–349, doi: 10.1016/S0009-2541(00)00418-6

Patriat P, Sauter D, Munschy M, et al. 1997. A survey of the Southwest Indian ridge axis between Atlantis II Fracture Zone and the Indian Ocean triple junction: regional setting and large scale segmentation. Marine Geophysical Researches, 19(6): 457–480, doi: 10.1023/A:1004312623534

Pluger W L, Herzig P M, Becker K P, et al. 1990. Discovery of hydrothermal fields at the central Indian ridge. Marine Mining, 9: 73–86

Rona P A, Klinkhammer G, Nelsen T A, et al. 1986. Black smokers, massive sulphides and vent biota at the Mid-Atlantic Ridge. Nature, 321(6065): 33–37, doi: 10.1038/321033a0

Sato T, Okino K, Sato H, et al. 2013. Magmatic activities on the Southwest Indian Ridge between 35°E and 40°E, the closest segment to the Marion hotspot. Geochemistry, Geophysics, Geosystems, 14(12): 5286–5307, doi: 10.1002/ggge.v14.12

Sauter D, Cannat M, Rouméjon S, et al. 2013. Continuous exhumation of mantle-derived rocks at the Southwest Indian Ridge for 11 million years. Nature Geoscience, 6(4): 314–320, doi: 10.1038/ngeo1771

Sauter D, Patriat P, Rommevaux-Jestin C, et al. 2001. The Southwest Indian Ridge between 49°15′E and 57°E: focused accretion and magma redistribution. Earth and Planetary Science Letters, 192(3): 303–317, doi: 10.1016/S0012-821X(01)00455-1

Scheirer D S, Baker E T, Johnson K T M. 1998. Detection of hydrothermal plumes along the Southeast Indian Ridge near the Amsterdam-St. Paul Plateau. Geophysical Research Letters, 25(1): 97–100, doi: 10.1029/97GL03443

Schmidt K, Koschinsky A, Garbe-Schönberg D, et al. 2007. Geochemistry of hydrothermal fluids from the ultramafic-hosted Logatchev hydrothermal field, 15°N on the Mid-Atlantic Ridge: temporal and spatial investigation. Chemical Geology, 242(1–2): 1–21, doi: 10.1016/j.chemgeo.2007.01.023

Seyler M, Cannat M, Mével C. 2003. Evidence for major-element heterogeneity in the mantle source of abyssal peridotites from the Southwest Indian Ridge (52° to 68°E). Geochemistry, Geophysics, Geosystems, 4(2): 9101

Smith D. 2013. Tectonics: mantle spread across the sea floor. Nature Geoscience, 6(4): 247–248, doi: 10.1038/ngeo1786

Son J, Pak S J, Kim J, et al. 2014. Tectonic and magmatic control of hydrothermal activity along the slow-spreading Central Indian Ridge, 8°S–17°S. Geochemistry, Geophysics, Geosystems, 15(5): 2011–2020, doi: 10.1002/2013GC005206

Standish J J, Sims K W W. 2010. Young off-axis volcanism along the ultraslow-spreading Southwest Indian Ridge. Nature Geoscience, 3(4): 286–292, doi: 10.1038/ngeo824

Tao Chunhui, Chen Sheng, Baker E T, et al. 2017. Hydrothermal plume mapping as a prospecting tool for seafloor sulfide deposits: a case study at the Zouyu-1 and Zouyu-2 hydrothermal fields in the southern Mid-Atlantic Ridge. Marine Geophysical Research, 38(1–2): 3–16, doi: 10.1007/s11001-016-9275-2

Tao Chunhui, Li Huaiming, Jin Xiaobing, et al. 2014. Seafloor hydrothermal activity and polymetallic sulfide exploration on the southwest Indian ridge. Chinese Science Bulletin, 59(19): 2266–2276, doi: 10.1007/s11434-014-0182-0

Tao Chunhui, Lin Jian, Guo Shiqin, et al. 2012. First active hydrothermal vents on an ultraslow-spreading center: southwest Indian Ridge. Geology, 40(1): 47–50, doi: 10.1130/G32389.1

Yang Weifang, Tao Chunhui, Li Huaiming, et al. 2017. $^{230}Th/^{238}U$ dating of hydrothermal sulfides from Duanqiao hydrothermal field, Southwest Indian Ridge. Marine Geophysical Research, 38(1–2): 71–83, doi: 10.1007/s11001-016-9279-y